A Numerical Study on Influences of Hurricane Gloria (1985) on the Environment

REBECCA J. ROSS* AND YOSHIO KURIHARA

Geophysical Fluid Dynamics Laboratory/NOAA, Princeton, New Jersey

(Manuscript received 21 January 1994, in final form 18 July 1994)

ABSTRACT

The influence of Hurricane Gloria (1985) on the environment is investigated by comparing hurricane model integrations either including or excluding the hurricane in the initial condition. Results for three cases of Gloria at different states of development are presented. The hurricane's cumulative influence is identified as the differences between the hurricane and nonhurricane integrations. Throughout the integration period, area with sea level pressure differences exceeding 1 hPa in magnitude expanded in each of the three cases and was centered at the hurricane location. The influence radius of the storm, which was determined from the sea level pressure difference field, eventually reached approximately 1500 km in all cases. Comparisons of the sea level pressure differences among the three cases showed that the expansion rate differed for each case but was only weakly related to the intensity or intensity change of the particular storm.

The comparisons of the wind and temperature fields from the hurricane and nonhurricane integrations indicated that the areal extent of the hurricane's influence was much larger at the upper layer than at the lower layer. A stronger anticyclonic circulation and relatively warmer temperatures developed at the upper layer in the hurricane integration compared to the nonhurricane fields. These upper-layer changes extended over an area comparable in size with the sea level pressure differences. These general features were identified in all three cases.

At the lower layer, the differences between the hurricane and nonhurricane wind and temperature fields showed the impact of hurricane on the passage of a cold front over the eastern United States. Apparently, the hurricane's cyclonic circulation at the lower layer affected the movement of the front approaching from the west. The frontal passage was delayed north of the storm in the hurricane integration because of the reduction in the eastward component of the wind. To the south of the hurricane, the westerly winds were enhanced to accelerate the front movement. There were related changes in the fields of precipitation and the low-level temperature; for example, southwest of the hurricane, there was a reduction in the accumulated frontal precipitation in the hurricane integration because of the faster frontal movement.

1. Introduction

An interesting and complex aspect of tropical cyclone forecasting is to determine the effects of interactions between the tropical cyclone and its environment. Examples of relatively straightforward interactions include the decay of a tropical cyclone after landfall or upon encountering colder sea surface temperatures. The synoptic-scale flow is also observed to influence the intensification or decay of tropical cyclones. Tropical cyclones typically weaken after entering regions of strong vertical wind shear. Molinari and Vollaro (1989) have linked the intensification of developing tropical cyclones to interactions with upper-troposphere vorticity maxima. Most studies along these lines consider only the modifications to the tropical cyclone due to the environment. In general, however, interaction implies influence in both directions; modifying the environment as well as the hurricane. Certainly, the passage of a hurricane has an enormous impact on the areas within the region of high winds and torrential precipitation associated with the eyewall. Farther from the storm center, the degree of the hurricane's influence on its environment is less intense and is more difficult to distinguish from general changes in the environment. What changes can be induced in the environmental flow as a result of the hurricane forcing?

A composite study by Frank (1982) of the western Pacific and West Indian tropical cyclones showed that the presence of mature tropical cyclones was identifiable out to 1600 km from the storm center. The strengthening of the upper-level anticyclone was the feature of the composite tropical cyclone with the strongest signal at this large radius. This study also considered the possible impact of tropical cyclone passage in terms of modifying the atmospheric environment either favorably or unfavorably for tropical cyclone genesis and development. The composite results suggested that vertical shear patterns of the environmental winds after the passage of tropical cyclones were favorable

* Current affiliation: Air Resources Laboratory/NOAA, Silver Spring, Maryland.

Corresponding author address: Dr. Yoshio Kurihara, NOAA/GFDL, Princeton University, Post Office Box 308, Princeton, NJ 08542.

for development of new tropical storms. Observational case studies considering the hurricane's influence in modifying the environmental flow are few, probably because of the difficulty in isolating the hurricane's effect in the evolving environmental flow. In this regard, three-dimensional numerical model integrations allow a controlled means of identifying the contributions of the hurricane to environmental flow changes.

The purpose of this study is to investigate the modifications to the environment resulting from the presence of the hurricane for three cases of an observed hurricane using the Geophysical Fluid Dynamics Laboratory (GFDL) hurricane model. The approach taken here is to compare two regional model forecasts from initial conditions that differ in the presence or absence of the hurricane. In each case the integration including the hurricane represents the realized fields, whereas the integration without the hurricane is assumed to represent the atmospheric evolution if the hurricane had not been present. The ability to predict the flow evolution without the hurricane is the advantage of the model-based approach compared to an observational case study. The differences in the evolution of the environment between the two integrations indicate the areal extent of the hurricane's influence with time over the limited-area model domain. Additionally, examples of modifications to particular features of the environment due to the presence of the hurricane are described. It should be emphasized that the effects of the hurricane on the environmental fields are certainly case dependent. The cases presented here suggest that the effects depend on the particular synoptic situations of the environmental flow and, also, possibly on conditions of the hurricane.

Hurricane forecasting has primarily focused on accurate forecasts of the hurricane track. As the skill of dynamical prediction models has improved it has become feasible to attempt forecasts of other quantities such as storm intensity, maximum low-level winds, and precipitation (Bender et al. 1993, hereafter referred to as BRTK). In forecasting these quantities the accurate prediction of the evolving three-dimensional structure of both the hurricane and its environment is essential. Clearly, the prediction of the hurricane is affected by its environment while the hurricane influences the prediction of its environment. The analysis of the magnitude and extent of the storm's impact is intended as a useful indication of the importance of the hurricane in affecting the accurate prediction of the surrounding environment.

Section 2 briefly reviews the GFDL hurricane prediction model and describes the three cases considered. Section 3 presents the experimental strategy for isolating the hurricane influence. The results of the model integrations are presented and discussed in section 4, and the summary and remarks are included as section 5.

2. Model and case description

The GFDL multiply nested movable mesh (MMM) model described by Kurihara and Bender (1980), with additional model details presented in Bender et al. (1987) and BRTK was used for the model forecasts described here. The primitive equation model is formulated in latitude, longitude, and sigma coordinates with 18 levels in the vertical (Table 1 of Kurihara et al. 1990). A triply nested grid system of resolutions 1°, $^1/_3$°, and $^1/_6$° was used over a domain of 75° latitude by 75° longitude and lateral boundary conditions were taken from the NMC T80 global forecasts as described in BRTK. The model physics included a cumulus parameterization described by Kurihara (1973), a Monin–Obukhov scheme for the surface flux calculation and the Mellor and Yamada (1974) level-2 turbulence closure scheme for vertical diffusion with a background diffusion coefficient added. Additionally, as described in Tuleya (1994), a diurnal radiation cycle was incorporated in the model along with land surface temperatures computed by an energy budget equation including a soil layer. However, interactive soil hydrology was not considered. The sea surface temperatures were held fixed to the initial distribution throughout the integration.

To maximize the likelihood of isolating a strong signal of hurricane impact on the environment, the three cases chosen here were based on Hurricane Gloria (1985), a large and intense hurricane. Each case represented a different stage in hurricane intensity, that is, the minimum surface pressure, and size. The case G22, initialized at 1200 UTC 22 September, began prior to the period of rapid intensification with an initial minimum sea level pressure (SLP) of 992 hPa for the model hurricane. Case G24 began on 0000 UTC 24 September during the period of rapid intensification with an initial minimum SLP of 961 hPa for the model hurricane. The third case, G25, began on 0000 UTC 25 September when Gloria was at maximum intensity with an initial SLP of 923 hPa.

For each of the three cases chosen, the MMM model forecasts were performed from two initial conditions: one with a hurricane (hurricane integration) and the other without a hurricane (nonhurricane integration). The initial conditions for all hurricane integrations were determined with the GFDL hurricane model initialization scheme described in Kurihara et al. (1993, hereafter referred to as KBR) by using the NMC T80 global analysis for the initial analysis input. As described in section 3, the initial condition for the nonhurricane integration of each case was obtained by removing the Gloria vortex from the corresponding initial condition for the hurricane integration. The model was integrated for 132 h (5.5 days) in case G22, for 96 h (4 days) in G24 and for 72 h (3 days) in G25. In the nonhurricane integration, the inner meshes of the nested mesh model were prescribed to move according

to the mesh movement in the corresponding hurricane integration. An important point is that both the hurricane and nonhurricane integrations use an identical model. The sensitivity of the model integration to changes in boundary conditions, soil hydrology, or sea surface temperature is not discussed in this study.

It should be noted here that the initial conditions for the hurricane integrations in this study differed slightly from the corresponding ones in BRTK due to recent small modifications in the model initialization technique. Also, the effect of radiation was better treated in the present model. For strong storms such as the present one, the above modifications have not caused any noticeable changes in the storm track prediction although storm intensity in the model was affected in the case of G24. The G25 hurricane integration showed little change from the realistic result of BRTK prediction and, therefore, the numerical results from the G25 case are the focus of most of the following analyses.

3. Experimental strategy

The experimental strategy taken in this study for isolating and identifying the impact of the hurricane on the environment is to compare two forecasts from initial conditions that differ only in the presence or absence of the hurricane. Although there exists a degree of arbitrariness in the separation of the hurricane, the forecast from the nonhurricane integration is assumed to represent the evolution of the atmospheric environment without the influence of hurricane. On the other hand, the environmental fields in the hurricane integration are affected continually by the presence of the hurricane. Accordingly, the differences between the hurricane and nonhurricane integrations in each case result from the cumulative impact of the hurricane's presence. Note that the experimental design used here is capable of showing only the impact of the hurricane on the environment. The differences between the two integrations at any time can be loosely partitioned into two domains. The first is the area in the immediate vicinity of the storm position (defined as the location of the storm's minimum SLP) and will be referred to as the storm domain. Differences in this region are characterized by strong gradients in winds or SLP and result directly from the presence of the hurricane at that location in the hurricane integration. The size or extent of the storm domain is somewhat arbitrary but for the purposes of this study will be taken to be equal to twice the radius of the outermost closed isobar at the surface. The second region is the remainder of the model grid domain beyond the storm domain. Differences in this region represent a less direct influence from the hurricane and show the changes in the environment that accumulate because of the continuing presence of the hurricane.

In addition to the comparison between the two integrations in each case, the comparisons among the three cases will indicate the relationship, if any, of storm intensity and intensity change to the extent of the hurricane impact on the environment. Also, because the prediction periods of the three cases overlap for the final 72 h of integration, the consistency among the impacts in the three cases for similar environments can be at least qualitatively checked.

In the present study, the hurricane vortex in the initial condition for the hurricane integration is removed to obtain the initial condition for the nonhurricane integration. Since the procedure of vortex removal is an important part of the present work, the vortex filtering scheme used is briefly described. For consistency with the model initialization of the hurricane integration as well as convenience, the vortex removal is performed by the filtering technique developed as part of the GFDL hurricane initialization scheme (see KBR for full details). There are two filtering steps, the first consists of the application of a simple local smoothing operator to all variables of the initial fields for the hurricane integration, splitting each into a large-scale field and a disturbance field. The second filtering step occurs over a cylindrical domain centered on the storm position and separates the disturbance field into a hurricane and a nonhurricane component. The radius of this domain represents the outermost extent of the hurricane vortex and in this case is known from the vortex generation process in the specification of the hurricane integration initial condition. Specifically, this radius is set as twice the reported radius of the outermost closed isobar at the surface, that is, the same as the radius of the storm domain defined before. The final procedure in creating the nonhurricane initial condition is the recombination of the large-scale field with the nonhurricane disturbance component to obtain fields representing the environment without the hurricane. The nonhurricane initial condition obtained by this filtering process was identical to the hurricane initial condition except within the local region of the hurricane (defined by the cylindrical domain radius). For the three cases used here, this radius ranged from 745 km for G22 to 960 km for G25.

Figure 1 shows the initial sea level pressure fields of G25 for the hurricane and nonhurricane integrations, respectively. Note the absence of the hurricane vortex in the latter. A characteristic of the KBR filtering scheme is the gradual scale separation over the range of scales where the distinction between hurricane and environment is less distinct. An important consideration in the design of the filtering scheme was to retain mesoscale or synoptic features near the storm in the generated initial condition. For example, in the nonhurricane field in Fig. 1 the remaining synoptic disturbance may represent the easterly wave in which Gloria was embedded.

As a further example of the removal of the hurricane, Fig. 2 shows the wind vectors at an upper layer of the model (average for $\sigma = 0.074-0.275$) for the hurricane

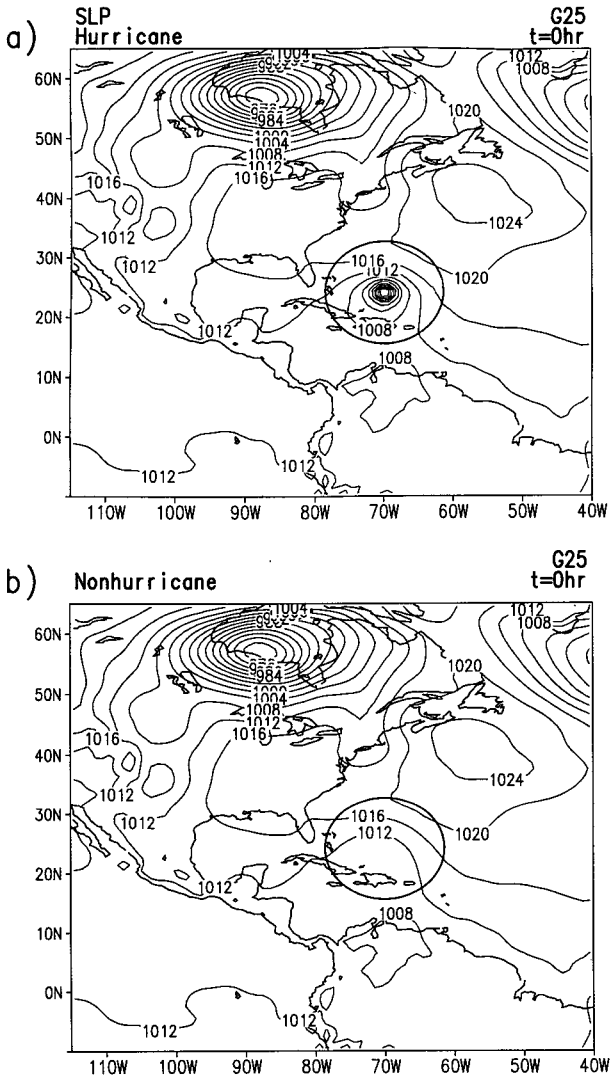

FIG. 1. Distribution of the sea level pressure (SLP) (hPa) at the initial time for case G25, that is, at 0000 UTC 25 September 1985, in (a) the hurricane integration and (b) the nonhurricane integration. The storm domain is encircled by a thick line.

and nonhurricane initial conditions. The anticyclonic circulation centered on the hurricane location in the hurricane initial condition has been removed to obtain the nonhurricane initial condition while surrounding features are retained. The initial hurricane in the hurricane integration is a vortex generated through the model initialization scheme (KBR) and exhibits expected hurricane circulation features such as a deep cyclonic circulation with low-level radial inflow and an upper-level anticyclonic circulation. However, it should be noted that the upper-level flow is probably less realistic than the lower-level flow because of conditions and constraints used in the vortex generation procedure. In particular, the hurricane is confined within the prescribed storm domain. It is likely that Hurricane Gloria's actual outflow at the time of maximum intensity (G25) extended beyond the storm domain of 960-km radius.

Because the removal of the hurricane is arbitrary to some degree, it is important to consider how the possible presence of some hurricane residual might affect the subsequent nonhurricane forecast. The most obvious result of insufficient filtering would be the development of a new hurricane disturbance in the nonhurricane integration. Clearly, this would indicate the need for stronger filtering of the hurricane initial condition. However, no disturbances developed in the nonhurricane integrations in the cases used here.

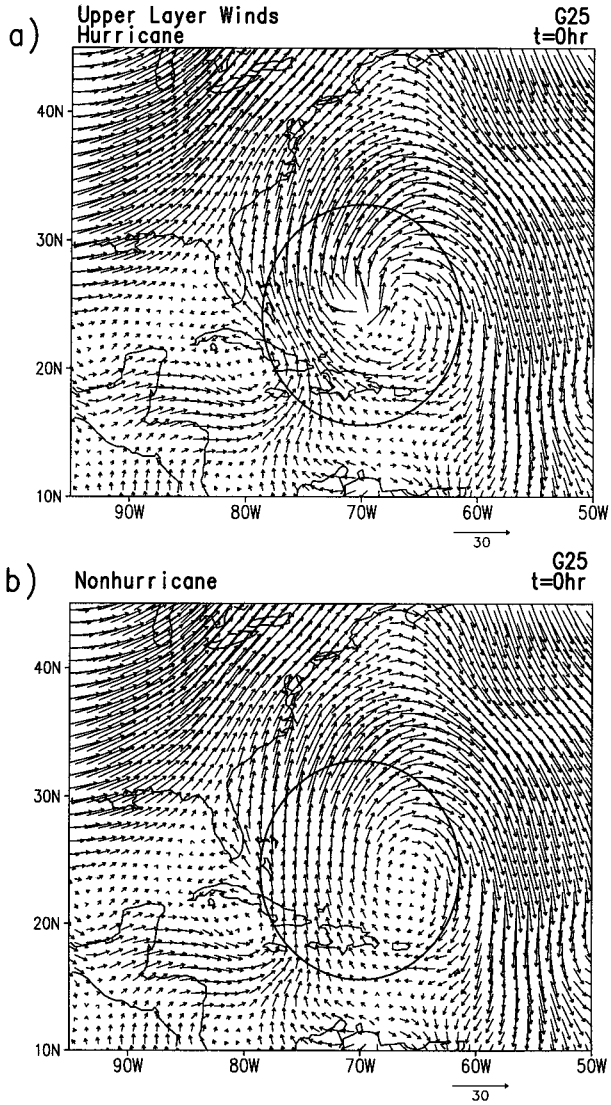

FIG. 2. Distribution of the upper-layer (σ = 0.074–0.275) winds (vector scale in meters per second) at the initial time for case G25, in (a) the hurricane integration and (b) the nonhurricane integration. The storm domain is encircled by a thick line.

Another issue is the sensitivity of the nonhurricane forecast to the vortex separation procedure. Because of the smoothness of the nonhurricane initial condition fields across the storm domain, it was expected that the subsequent evolution of the environment would be primarily driven by the synoptic-scale features outside of the storm domain and would be relatively insensitive to small changes in the fields within the storm domain resulting from different filtering procedures. This supposition was tested by integrating the model from a second nonhurricane initial condition for case G25 with minor alterations to the filtering parameters. The initial differences in SLP between the two nonhurricane initial conditions were of course much smaller (maximum difference of 0.8 hPa) than those due to the presence of a hurricane. After 60 h of integration, distribution of SLP differences was not coherent and was confined mostly to the Atlantic coastal region. The differences had a maximum absolute value of 2 hPa but were mostly less than 1 hPa. In the presentation of the SLP differences between the hurricane and nonhurricane integrations in section 4, differences less than 1 hPa will be considered as noise. Similar comparisons for wind speed and temperature differences indicate that 3 m s^{-1} and 1 K are appropriate noise estimates for these variables.

4. Results

a. *Spreading of the hurricane influence*

The three cases presented here all involved a storm that was already of hurricane strength and thus some environmental modification due to the presence of the storm should have occurred prior to the initial times of the model integrations. In this respect, the differences between the hurricane and nonhurricane integrations would represent a lower bound, especially at the initial time and in an early period of the integrations, on the extent of the hurricane impact. Additionally, some residual of the broad and relatively weak vortex that existed in the NMC global analysis may be present in the initial conditions if this vortex is not entirely removed with the model initialization scheme used. However, any such residual equally exists in both the hurricane and nonhurricane initial conditions and is thus considered part of the environment. The evolution of differences between the two integrations are designed to indicate how the hurricane progressively affects the environment from the initial time.

Figure 3 shows the difference between the hurricane and nonhurricane initial conditions for the fields of SLP and the upper-layer radial wind computed relative to the storm position for case G25. The initial condition differences are associated with the presence and structure of the hurricane vortex generated through the KBR initialization procedure. The negative differences of SLP were centered on the hurricane position and represent the substantial negative deviation of pressure of the tropical cyclone from the background environment. The radial wind differences are predominantly positive and represent the outflow of the tropical cyclone. The initial condition differences were smaller in magnitude for cases G22 and G24, reflecting the weaker stages of the hurricane at those initial times. Also the areal extent of the initial condition differences was largest for the strongest case G25. The weakest case, G22, had initial condition SLP differences exceeding 1 hPa in magnitude over an area of 29.4 $\times$ 10^4 km^2 compared with 68.1 $\times$ 10^4 km^2 for G24 and 121.8 $\times$ 10^4 km^2 for G25. These areas correspond in size to circles with radii 306, 466, and 623 km, respectively. In the present study, such a radius will be referred to as the influence radius

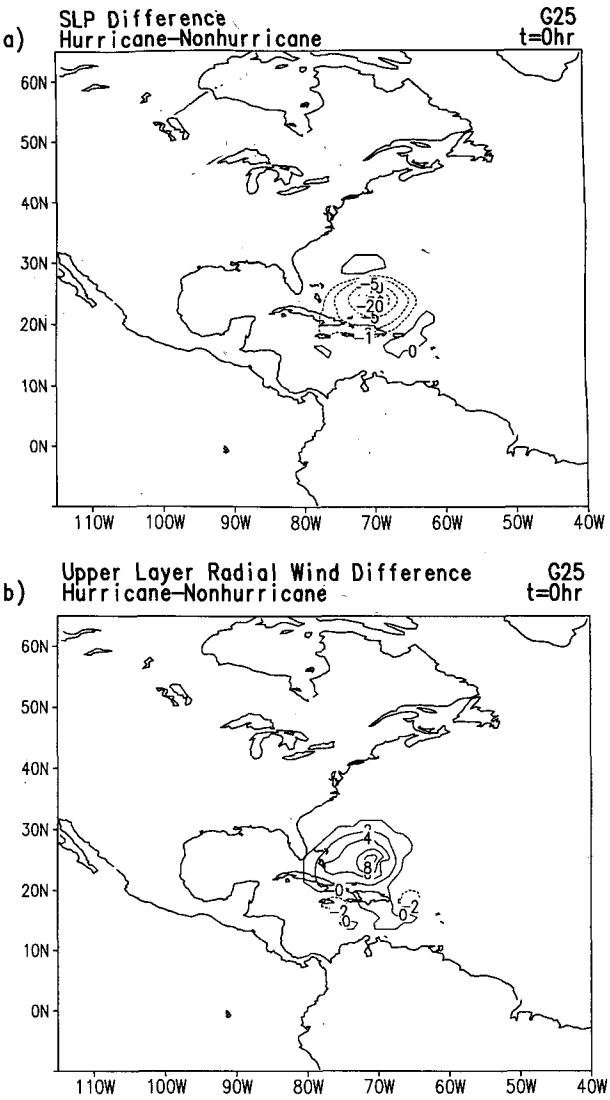

FIG. 3. Distribution of the differences (hurricane minus nonhurricane) in (a) the sea level pressure (hPa) and (b) upper-layer (σ = 0.074–0.275) radial wind (m s^{-1}) at the initial time for case G25.

of the storm (IRS), more exactly its lower bound as mentioned before. Note that, due to the choice of a particular threshold value for determining the SLP difference area, the IRS will be smaller than the radius of the storm domain until the hurricane influence significantly spreads.

Over the integration period for each case, the differences in the prognostic variables (wind, temperature, mixing ratio of water vapor, and surface pressure) between the hurricane and nonhurricane integrations grew in areal extent beyond the storm domains. The fields of SLP after 60 h of the hurricane and nonhurricane integrations in case G25 are shown in Figs. 4a and 4b. The determination from Fig. 4a of storm size (as twice the radius of the outermost closed isobar) at this time yields a radius of approximately 950 km. The storm domain defined by this radius is indicated by the circle on Figs. 4a and 4b and, in Fig. 4a, completely contains the strong pressure gradients associated with the hurricane's pressure minimum. Beyond this domain, an increase in the curvature of the 1016- and 1020-hPa isobars to the east and northeast of the storm is apparent in the hurricane integration, and the lower SLP there suggests a broader influence from the hurricane's cyclonic circulation. Lower pressure in the hurricane integration also exists to the west and southwest of the hurricane. However, this feature is not obvious without comparison to the corresponding field in the nonhurricane integration. Such an identification of subtler impacts resulting from the hurricane's presence and well beyond the storm domain is the strength of this experimental strategy.

The SLP differences corresponding to the G25 fields in Fig. 4 are shown in Fig. 5a. There is of course an area of large negative differences centered on the storm that reflects the presence/absence of the hurricane in the integration pair. Certainly, beyond the circle representing the storm domain the negative SLP differences are still discernible and extend over 2000 km from the storm center in the west to east direction. A region of positive SLP differences is located north of the storm center over Hudson Bay. Comparison with Fig. 4 shows that the positive differences represent enhanced deepening of the trough in the nonhurricane integration compared with the hurricane integration.

In contrast, the SLP difference after 60 h of the G22 integration pair is shown in Fig. 5b. The location of the hurricane is again easily seen. In this case, the storm domain radius at this time is approximately 750 km and is indicated by the circle in Fig. 5b. Unlike the G25 case, the SLP differences less than -1 hPa are mostly confined to a rather small area surrounding the storm. The corresponding difference field for G24 (not shown) is similar in extent to that of G22. For comparison, the areal coverage of SLP differences less than 1 hPa is 256.7×10^4 km^2 (IRS = 904 km) for G22, 214.8×10^4 km^2 (IRS = 827 km) for G24, and 689.8×10^4 km^2 (IRS = 1482 km) for G25 after 60 h of

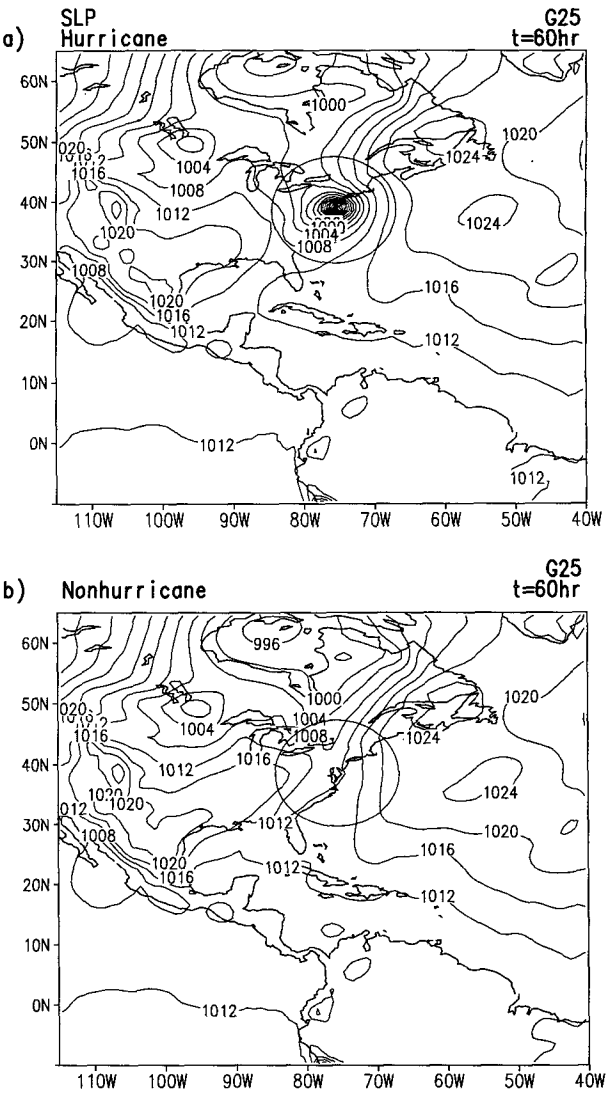

FIG. 4. Distribution of the sea level pressure (SLP) (hPa) after 60 h of (a) the hurricane integration and (b) the nonhurricane integration for case G25. The storm domain is encircled.

integration. Clearly, in the first 60 h of case G22, the hurricane influence on the environment was limited to the immediate area of the storm (904-km IRS vs 750-km storm domain). However, the spreading impact from the strong initial storm of case G25 was extensive enough by 60 h to have noticeably affected a large area of the surrounding environment (1482-km IRS vs 950-km storm domain).

The areal expansion of the SLP differences during the entire integration period for the three Gloria cases is examined in relation to the storm evolution. The 12-hourly IRS values for the three cases are listed in Table 1. The initial IRS value in cases G24 and G25 was smaller than that of G22 for the corresponding time (466 km vs 568 km and 623 km vs 904 km) in spite

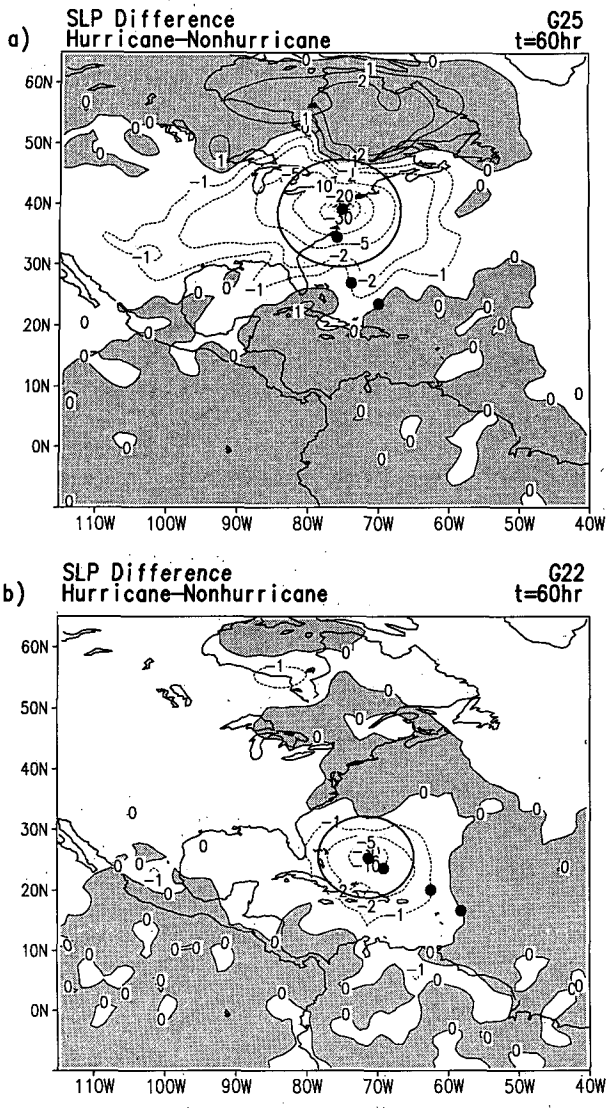

FIG. 5. Distribution of the differences (hurricane minus nonhurricane) in the sea level pressure (hPa) after 60 h of integration for (a) case G25 and (b) case G22. Contour levels are −30, −20, −10, −5, −2, −1, 0, 1, 2, and 4 hPa. Positive differences are shaded. The storm domain is encircled. Black circles indicate the storm position at 0, 24, 48, and 60 h.

of the small expansion of SLP differences noted in Fig. 5b at 60 h for G22. This supports the earlier suggestion that the hurricane had probably influenced the environment prior to the start of each integration. The IRS values continuously increase over the integration period in each case, reflecting the cumulative effect of the hurricane's presence. By the end of the integrations (i.e., at 0000 UTC September 28) the storm influence radii estimated from the SLP differences had expanded to 1427, 1483, and 1507 km, respectively, in G22, G24, and G25. Those final IRS values are quite similar given the different length of integration periods for each case (72–132 h).

The rate of expansion of the IRS is different for each of the three cases. For example, the length of time before the IRS exceeded the storm domain radius was just over 24 h for G25 (IRS ≈ 950 km), whereas case G22 required approximately 48 h (~750 km) and G24 required 60 h (~850 km). Additionally, the rate of expansion for each case was not constant throughout the integration. Shown in Fig. 6 are the time series of the rate of the IRS change (upper panel) and the model-predicted tropical cyclone minimum surface pressure (lower panel) for the three cases. The intensity changes in the hurricanes in G22 and G25 roughly agreed with the observed change. In contrast, the G24 forecast did not intensify as was observed. In G25, the storm influence most vigorously expanded after 12 h and the IRS increase reached a peak rate of 19.5 km h^{-1} at 36 h. Case G22 expanded more rapidly after 36 h when the model storm was rapidly deepening but the rate of expansion dropped below 10 km h^{-1} by 60 h even though the minimum surface pressure remained fairly intense. Case G24 was a case of relatively slow spreading in a relatively weak storm over the first 48 h. However, the expansion rate of G24 significantly increased after that time despite little corresponding change in the minimum surface pressure. The above comparison suggests that the relationship, if any, between the rate of expansion of the IRS and the intensity of the hurricane is rather inconsistent.

The above results indicate that the storm can eventually affect the environment at a substantial distance from the storm center. Such an impact of the storm can be important for the prediction of the large region surrounding the storm. However, the extent of the impact clearly varies from case to case as the SLP differences of Fig. 5 show. Note that the differences in the G22 and G25 extent in Fig. 5 may result from the different environments and/or the different representations of the storm (i.e., size and intensity). The qualitative agreement in the IRS values of Table 1 over the last 48 h of integration suggests a controlling influence of the environment on the extent of the hurricane's impact. It is possible that this is related to environmental

TABLE 1. Influence radius of the storm (km).

Verifying time	G22	G24	G25
1200 UTC 22 September	306		
0000 UTC 23 September	432		
1200 UTC 23 September	534		
0000 UTC 24 September	568	466	
1200 UTC 24 September	754	575	
0000 UTC 25 September	904 (60 h)	598	623
1200 UTC 25 September	922	688	703
0000 UTC 26 September	1012	773	900
1200 UTC 26 September	1113	827 (60 h)	1104
0000 UTC 27 September	1187	1038	1369
1200 UTC 27 September	1331	1222	1482 (60 h)
0000 UTC 28 September	1427	1483	1507

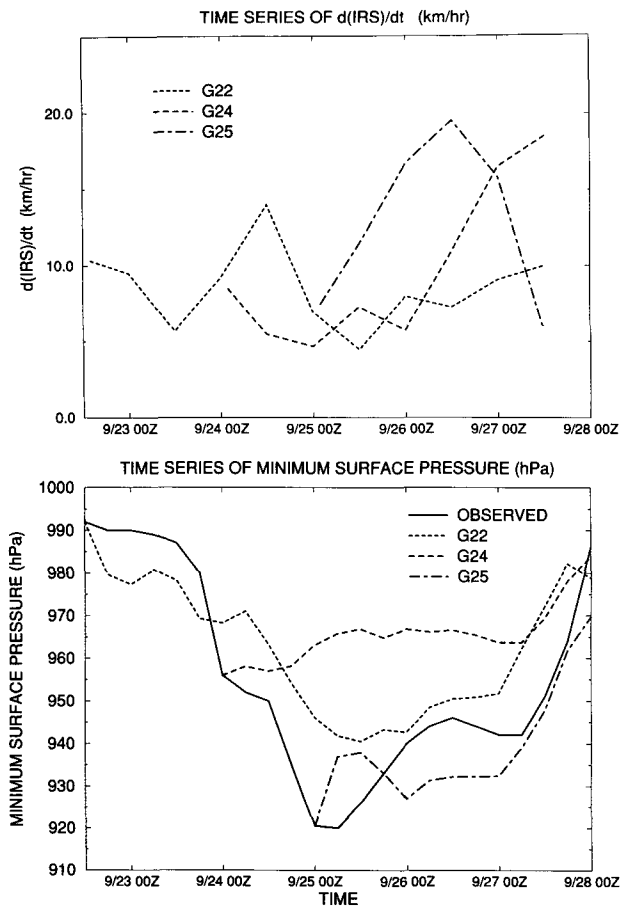

FIG. 6. Time series of the rate of change of the influence radius of the storm (IRS) (km h^{-1}, upper panel) and that of the hurricane minimum surface pressure (hPa, lower panel) for cases G22, G24, and G25. The observed minimum pressure is also plotted.

influences on the hurricane's evolution but this speculation cannot be investigated with the experimental strategy of this study.

It should be noted that the SLP difference pattern tended to remain centered (i.e., largest differences occurred) at the hurricane location throughout the model integration period as the hurricane progressed along its track. The magnitude of the SLP difference at any particular point rapidly decreased as the storm moved northward leaving little apparent lingering influence or aftereffect. This feature is seen in Fig. 5 in which the G25 storm positions at hours 0, 24, 48, and 60 are marked by black circles on the field of SLP difference. No clear signal indicating the storm's track was left behind. Thus, the memory of the storm passage in the SLP was not discernible. Note that this model did not include mechanisms for the interactive change of either SST or soil moisture, that is, two variables having possibly longer time constants with respect to the effects of hurricane passage.

b. Characteristics of influences at hour 60 for case G25

The SLP differences are a convenient single-level field for assessing the overall horizontal extent of the hurricane's influence. To identify the characteristics of the spreading influence in more detail, however, it is necessary to consider the three-dimensional structure of the modeled atmosphere. For this purpose, the conditions of the hurricane and nonhurricane integrations at hour 60 for case G25 were investigated.

As mentioned in section 3, the hurricane in the initial condition contains the radial wind (i.e., low-level inflow and upper-level outflow) that is a well-known feature of hurricanes. The upper-level outflow would seem to be an obvious mechanism to transport hurricane influences beyond the storm domain. On the other hand, the low-level inflow of the hurricane might be expected to yield changes that are more localized to the storm. Effects such as these are examined by comparing the wind and temperature fields of the hurricane and nonhurricane integrations at both upper and lower layers of the atmosphere.

Figure 7 shows the distribution of wind vectors averaged over an upper layer ($\sigma = 0.074-0.275$) for each integration. The dominant feature in both plots is the anticyclonic flow over the western Atlantic. The presence of the hurricane resulted in a shift of the center of anticyclonic circulation to the northwest (closer to the hurricane). The wind associated with the anticyclonic circulation is considerably stronger for the hurricane integration particularly on the north and east sides of the circulation. It seems the stronger winds on the southeast side of the circulation in the hurricane integration have enhanced a small cyclonic circulation centered at 20°N, 57°W. The position of this center shifted to the southwest from that of the nonhurricane integration. Over the northeastern portion of North America, the winds are also stronger in the hurricane integration and are directed more northward than in the nonhurricane integration. This is consistent with the addition of the upper-layer anticyclonic circulation of the storm in the hurricane integration. It may be speculated that the development of the upper-layer anticyclonic flow is associated with the continuing spread of the hurricane's influence throughout the integration.

The winds averaged over a lower layer ($\sigma = 0.777-0.995$) are shown in Fig. 8 for both the hurricane and nonhurricane integrations. The closed pattern and increased curvature of the wind speed contours surrounding the storm position for the hurricane integration show the presence and approximate extent of the storm. In the hurricane integration, the lower-layer wind vectors over the central United States have a more northerly component than those of the nonhurricane integration consistent with the presence of the cyclonic circulation. Along the Atlantic coast and southwest of the storm the flow has a stronger eastward component in

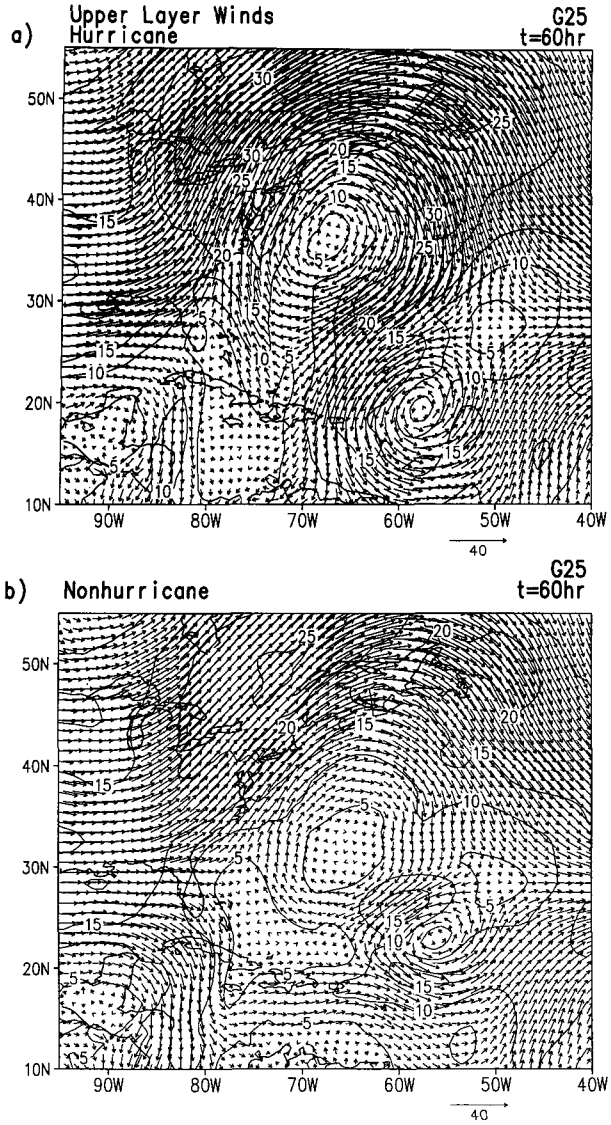

FIG. 7. Distribution of the upper-layer (σ = 0.074–0.275) winds (wind speed contour and vector scale in meters per second) after 60 h of (a) the hurricane integration and (b) the nonhurricane integration for case G25.

the hurricane integration as it is accelerated in toward the center. Also, the flow is stronger over Florida and the eastern Gulf of Mexico in the hurricane integration. On the other hand, the nonhurricane flow in Fig. 8b is characterized by a strong southerly flow north of Hispaniola and eastern Cuba. North of the hurricane's position, the wind vectors in the hurricane integration are directed to the northwest before they recurve to the northeast further downstream. The nonhurricane flow is consistently southwesterly in this region.

To show the extent of the storm's impact on the wind field, the wind speed differences between the hurricane and nonhurricane wind fields are presented in Fig. 9 at both the upper and lower layers. It is clear from Fig. 9a that the difference, mostly positive, spreads to a large region comparable in size with the domain of negative SLP difference (Fig. 5a). The effect of the storm on the lower-layer wind speed is strong and centered at the storm location, but the influenced area is smaller than that of the upper layer. Accordingly, the shaded area indicating the speed difference greater than 5 m s^{-1} is much smaller at the lower layer than the corresponding area for the upper.

The larger impact of the hurricane at the upper layer suggests that the G25 SLP differences (Fig. 5a) are linked to changes in the upper-layer anticyclonic cir-

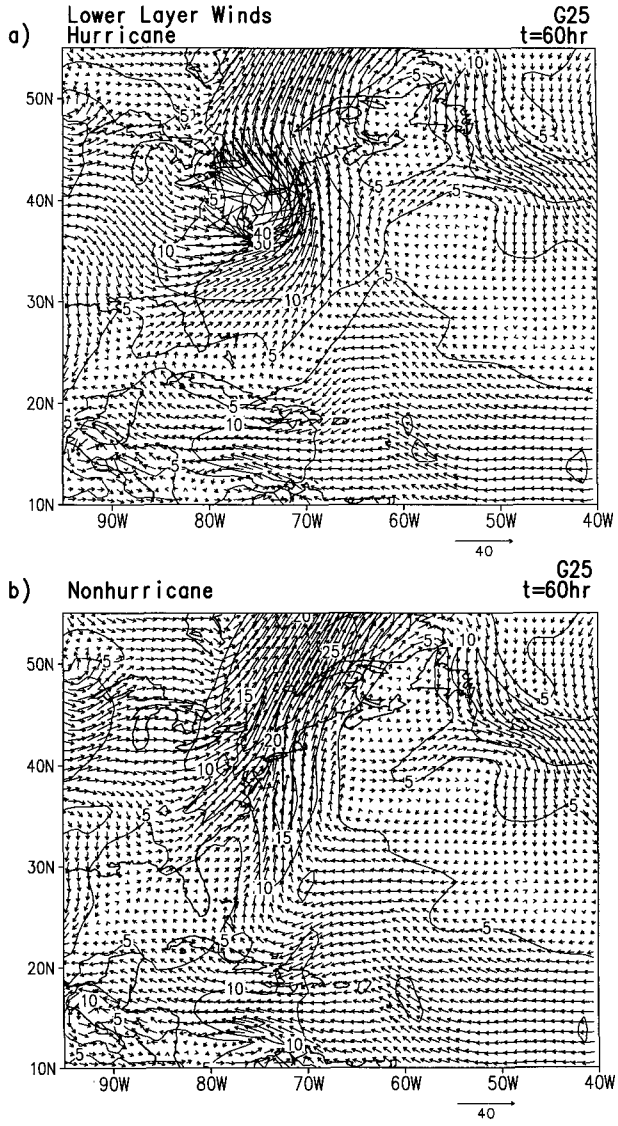

FIG. 8. Distribution of the lower-layer (σ = 0.777–0.995) winds (wind speed contour and vector scale in meters per second) after 60 h of (a) the hurricane integration and (b) the nonhurricane integration for case G25.

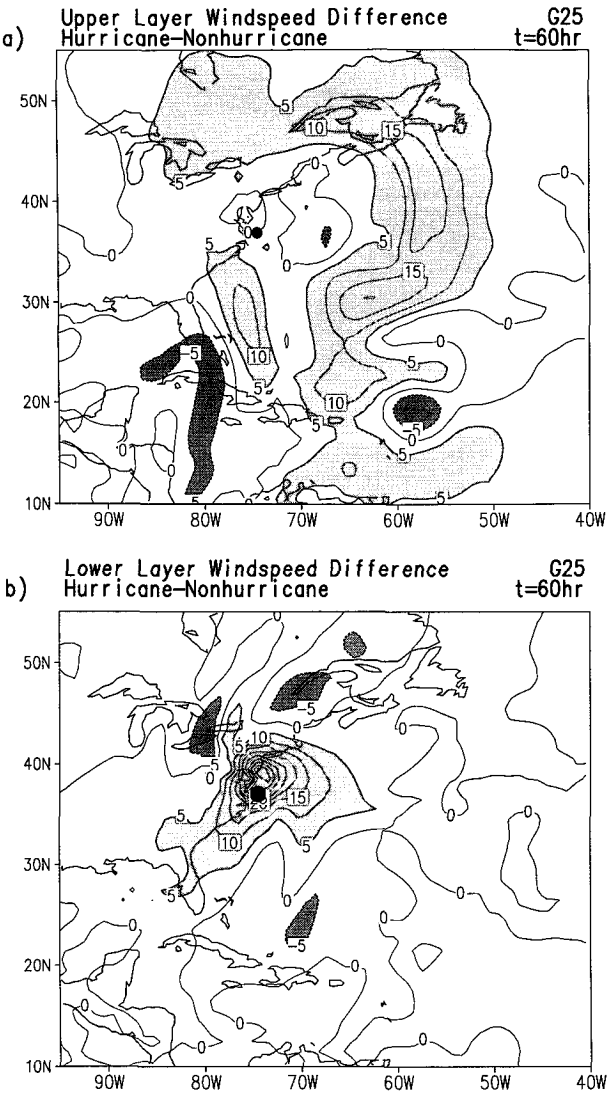

FIG. 9. Distribution of the differences (hurricane minus nonhurricane) in (a) the upper-layer (σ = 0.074–0.275) wind speed (m s^{-1}) and (b) the lower-layer (σ = 0.777–0.995) wind speed (m s^{-1}) after 60 h of integration for G25. Areas with the difference exceeding 5 m s^{-1} in magnitude are shaded.

culation resulting from the hurricane's presence. Further support for this relationship is seen by comparing the extent of SLP differences in case G22 with the corresponding upper-layer impact. The smaller extent of SLP differences in case G22 at 60 h (Fig. 5b) is associated with upper-layer wind speed differences covering a relatively small area as shown in Fig. 10a. On the other hand, the G22 upper-layer wind speed differences at 120 h (Fig. 10b) are much more extensive, consistent with the increase in the area of SLP differences represented by the IRS values in Table 1 (904 km at 60 h and 1331 km at 120 h). The wind speed differences at 120 h for G22 are for the same verifying time (1200 UTC September 27) as the 60 h G25 wind speed differences shown in Fig. 9a. Although the G22 differences are somewhat smaller than those of G25 (5–10 m s^{-1} compared with 10–15 m s^{-1}), the general pattern is quite similar. The closer agreement of the G22 and G25 differences at the same verifying time than after an equal length of integration time suggests that these differences represent evolving systematic modifications in the environment because of the hurricane's presence rather than the random diverging of the hurricane integrations from the nonhurricane integrations.

The differences in the temperature fields between the two integrations are shown in Fig. 11. The upper-layer

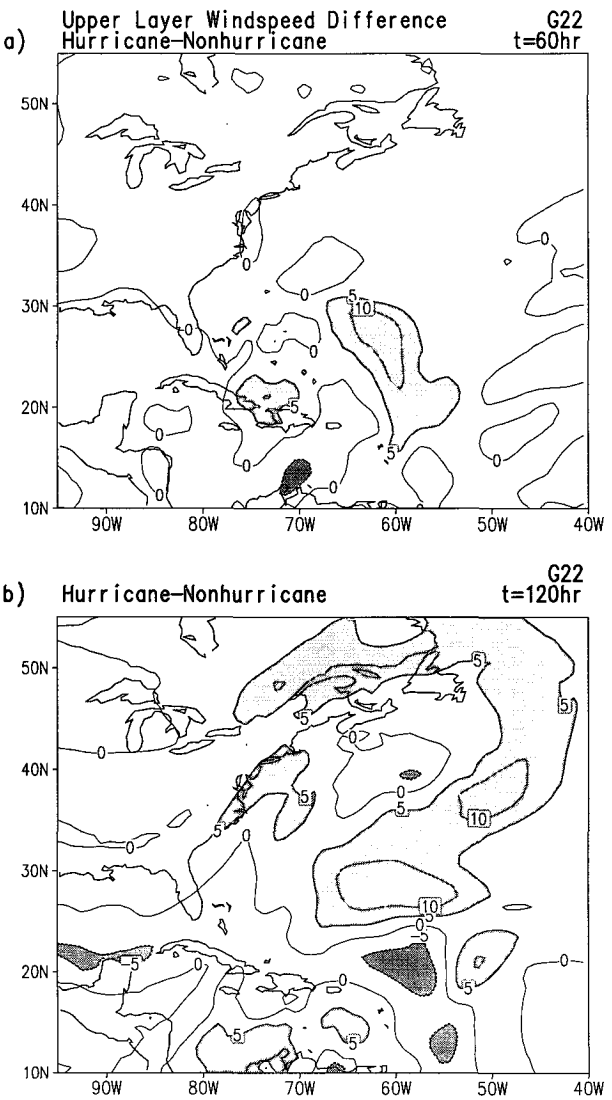

FIG. 10. Distribution of the differences (hurricane minus nonhurricane) in the upper-layer (σ = 0.074–0.275) wind speed (m s^{-1}) for case G22 after (a) 60 h and (b) 120 h of integration. Areas with the difference exceeding 5 m s^{-1} in magnitude are shaded.

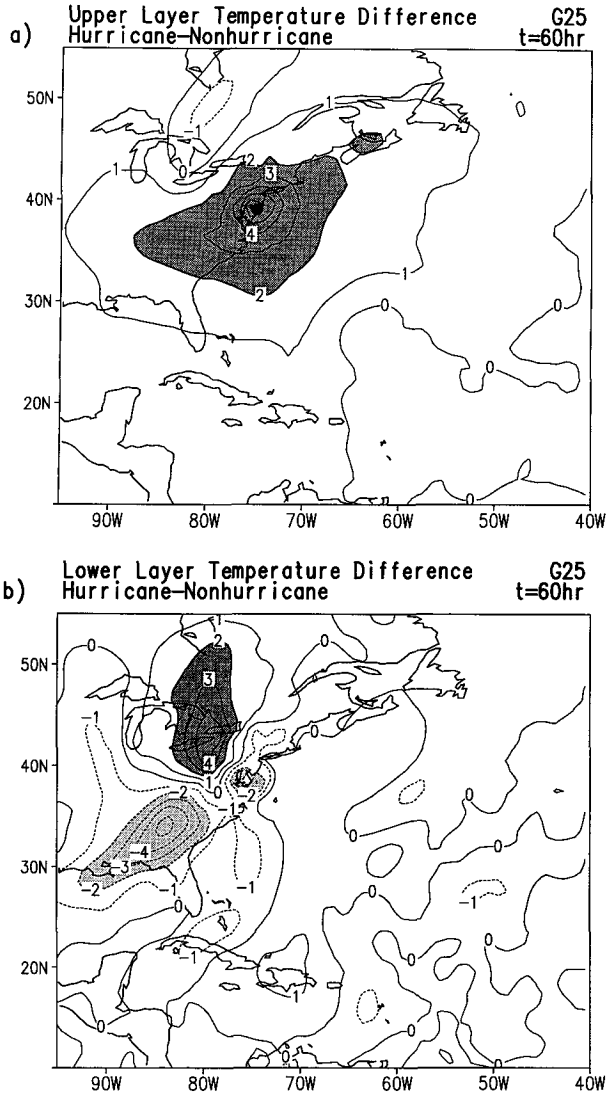

FIG. 11. Distribution of the differences (hurricane minus nonhurricane) in (a) the upper-layer (σ = 0.074–0.275) temperature (K) and (b) the lower-layer (σ = 0.777–0.995) temperature (K) after 60 h of integration for G25. Areas with the difference exceeding 2 K in magnitude are shaded.

temperature differences (Fig. 11a) are predominantly positive, suggesting that warmer air is exported from the hurricane to the environment over a substantial area. The affected area is roughly comparable in size to the area of negative SLP difference (Fig. 5a). Weak subsidence of the air may have contributed to the warming as well. The lower-layer temperature differences in Fig. 11b show that the area modified by the hurricane's presence at the lower layer is much smaller than at the upper layer. The area of negative differences over the southeastern United States at the lower layer indicates the temperature in the hurricane integration was colder than the nonhurricane integration. On the other hand, northwest of the hurricane position, the positive differences show that the hurricane integration was substantially warmer than the nonhurricane integration over the eastern Great Lakes. The combination of the upper- and lower-layer temperature differences implies that the vertical stratification of the atmosphere is more stable in the hurricane integration over the southeastern United States but less stable over the Great Lakes. The temperature differences in these two regions seem to be related to the passage of a cold front and will be further discussed in section 4d.

c. *Influence on the deep-layer mean wind*

As was shown in the preceding subsection, the presence of the hurricane had a noticeable impact on the meteorological conditions over a large domain surrounding the hurricane. An interesting implication of such an environmental modification is the possibility that hurricane-forced changes to the environment may subsequently affect the hurricane. Although the present experimental strategy is not appropriate for a direct investigation of this problem, it is still possible to make a slight suggestion that the hurricane-forced environmental change might affect the hurricane movement.

As a first-order approximation, it is supposed that the hurricane movement is dependent on the large-scale current at the storm location, that is, on the so-called steering current. Conventionally, the steering current is derived from the deep-layer mean of the winds in an area centered at the storm. In this respect, the deep-layer mean wind is a basic quantity related to the prediction of the storm motion. Application of the deep-layer mean wind to the storm-track forecast requires determination of an appropriate depth for taking the vertical average of the wind and formulation of a scheme to filter the steering current from the deep-layer mean wind field. However, these are problems beyond the scope of the present study.

In the present study, the deep-layer mean winds from the hurricane and nonhurricane integrations at hour 60 for case G25 are compared. It can be expected from the wind analysis as previously illustrated in Figs. 7, 8, and 9 that the deep-layer mean winds will show the upper- (lower-) layer signal of hurricane impact, to a reduced degree, at a region far from (near) the storm. Figure 12 shows the hurricane and nonhurricane deep-layer mean winds (averaged for the entire depth of the atmosphere). Note that the position shift and the difference in the strength of the anticyclonic flow over the western Atlantic between the two integrations are less in the deep-layer mean wind field as compared with those for the upper layer (Fig. 7). Nevertheless, there is an identifiable change in the general direction of the deep-layer mean wind over the storm area. Specifically, in the hurricane integration the general direction is nearly northward there, whereas in the nonhurricane integration it was toward the northeast. Such a differ-

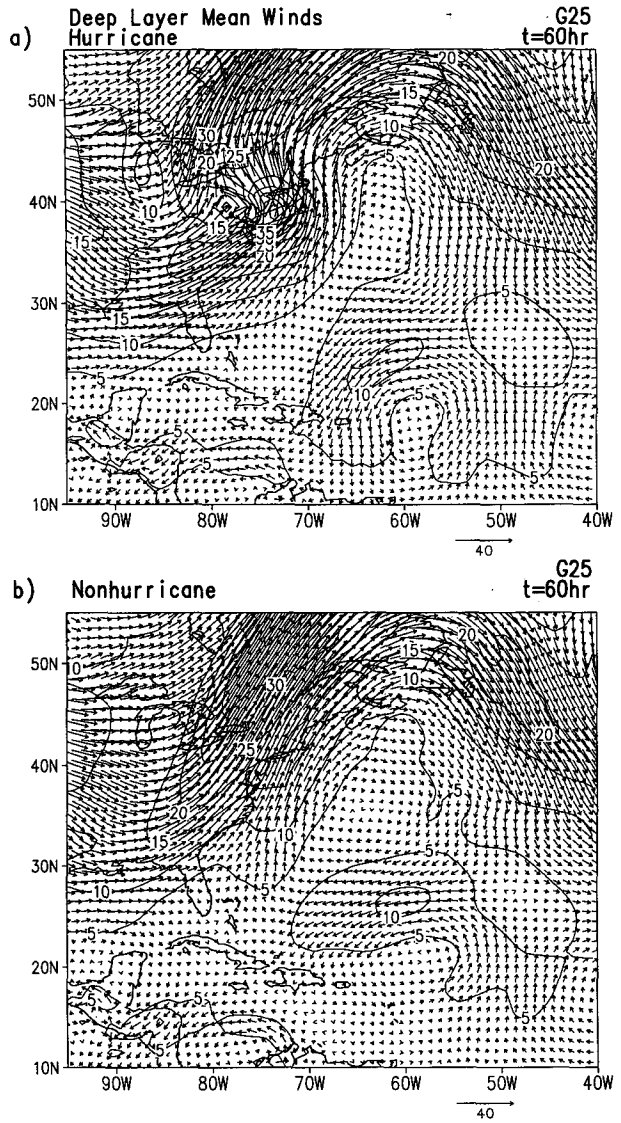

FIG. 12. Distribution of the deep-layer mean winds (wind speed contour and vector scale in meters per second) after 60 h of (a) the hurricane integration and (b) the nonhurricane integration for case G25.

ence in the deep-layer mean wind direction may affect the movement of the storm. In that case, it can be argued that the impact of the hurricane on the environment leads to a feedback influence on the storm. Results from a recent study using potential vorticity analysis (Wu 1994, personal communication) suggest that there are such cases.

d. Influence on a front

With the present experimental design it was possible to identify changes in the evolution of specific synoptic features that resulted form the presence of the hurricane. An example of this occurred to the west of the hurricane where a cold front advanced across the eastern half of the United States was eventually combined with the hurricane during the final day of the storm. The front separated the warmer and more moist air to the east from the colder and drier air mass to the west. The contrast between the two air masses can be seen in Fig. 13 showing the lower-layer average (σ = 0.777–0.995) mixing ratio of water vapor for each integration at 60 h in case G25. In both panels of Fig. 13 there is a sharp gradient in the mixing ratio over the eastern United States.

The environmental flow at this time was southwesterly east of the front and the hurricane circulation added

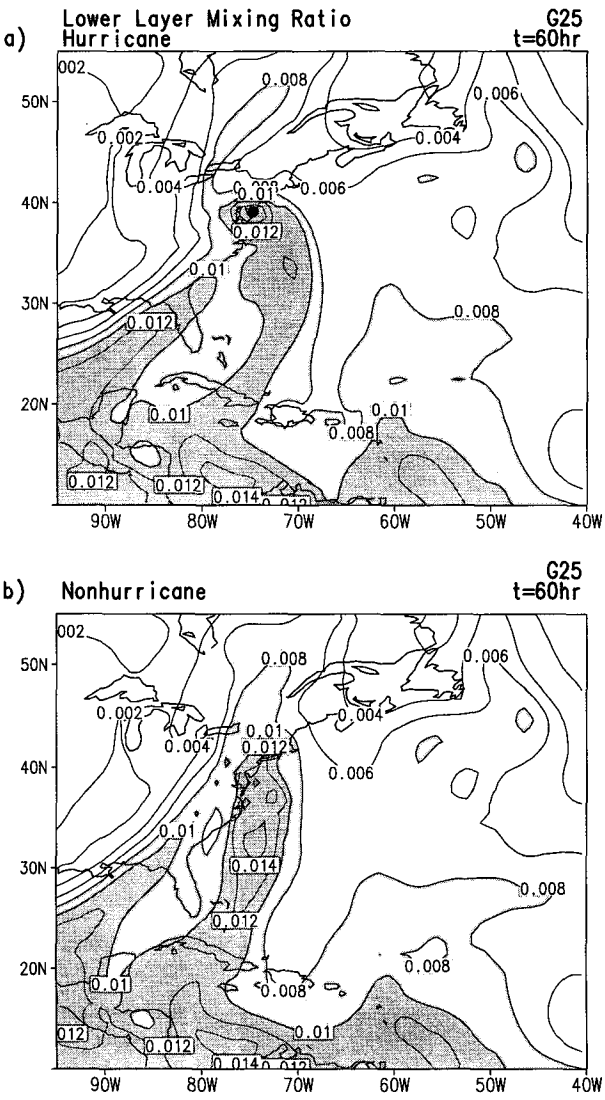

FIG. 13. Distribution of the lower-layer (σ = 0.777–0.995) mixing ratio of water vapor after 60 h of (a) the hurricane integration and (b) the nonhurricane integration for case G25. Shadings indicate areas above 8 g kg^{-1} (light shade) and 12 g kg^{-1} (dark shade).

an easterly component to the north of the storm and a westerly component to the south of the storm (Fig. 8). Thus, the influence of the hurricane to the north of the storm position was to decrease the eastward component of wind, leading to slowing of the eastward progress of the front. To the south of the hurricane, the westerly component of the wind was increased and the frontal passage was effectively accelerated in the hurricane integration. The accelerated frontal passage can be seen by comparing the mixing ratio fields for the hurricane and nonhurricane integrations in Fig. 13. Namely, the moist area just east of the front shown by darker shading in Fig. 13a crosses Florida and lies along the Atlantic coastline, while the corresponding moist area in Fig. 13b is still west of Florida and the coastline. The faster advance of the colder, drier air in the hurricane integration was probably responsible for the colder lower-layer temperatures over the southeastern United States relative to the nonhurricane integration previously shown in Fig. 11. The other moist zone extending from Cuba northward to the hurricane location is displaced to the east in the presence of the hurricane. Note that this moist zone is drier in the hurricane integration than in the nonhurricane integration (10 g kg^{-1} vs 12–14 g kg^{-1}), apparently because the hurricane's strong inflow caused convergence of the moisture into the storm's eyewall region. North of the hurricane's position the low-level flow in the hurricane integration has drawn much drier air over New England compared with the nonhurricane integration.

The changes in the temperature, wind, and mixing ratio fields, due to the influence of the hurricane, also resulted in changes in the precipitation pattern beyond the storm domain. Figure 14 depicts the 12-h (from 48 to 60 h) accumulated precipitation in each of the integrations. To the northwest of the hurricane, a larger area of accumulated precipitation greater than 0.2 cm (Fig. 14a) is consistent with the slower passage of the front as well as the less stable stratification. To the southwest of the hurricane, a reduction of precipitation there in the hurricane integration is in accordance with the accelerated frontal passage and the more stable stratification. In the nonhurricane integration, a slower movement of the front produced a more continuous band of precipitation that extended to the Gulf of Mexico. The nonhurricane integration also yielded a band of weak precipitation extending south-southeast of the hurricane location. This precipitation was apparently due to the abovementioned belt of moist southerly flow and the convergence of the low-level winds. By comparison, this area was drier and less convergent in the hurricane integration.

The hurricane influenced the cold front, though weaker, in cases G22 and G24. In both cases the frontal passage was accelerated south of the hurricane location and retarded to the north. The effects of these hurricanes on the precipitation were also qualitatively similar with those of G25. The most consistent feature for

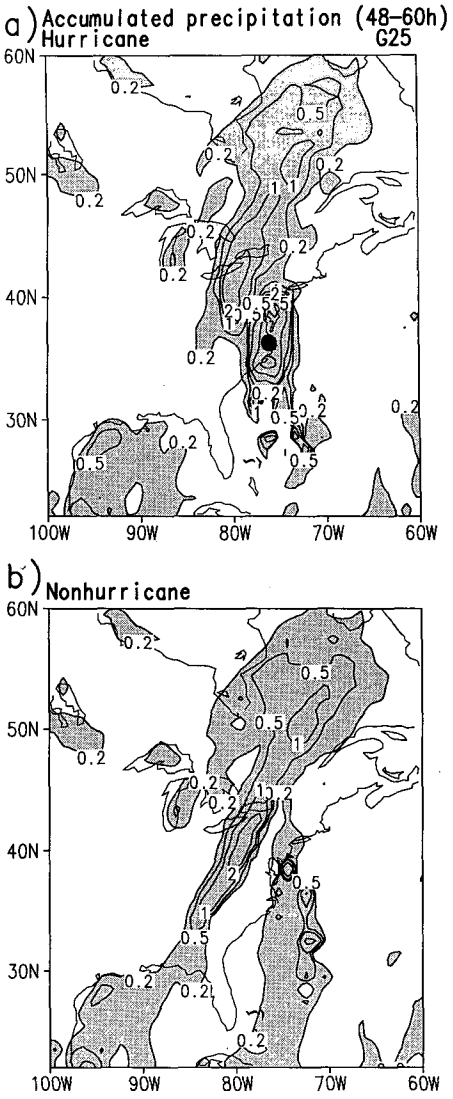

FIG. 14. Accumulated precipitation (cm) over the 12-h period (hour 48–hour 60) for (a) the hurricane integration and (b) the nonhurricane integration of case G25. Contour levels are 0.2, 0.5, 1, 2, and 5 cm. Areas above 0.2 cm are shaded. The solid circle in (a) represents the hurricane position at 54 h.

all cases was the presence (absence) of a precipitation band exceeding a certain amount along the cold front southwest of the hurricane location in the nonhurricane (hurricane) integration.

5. Summary and remarks

The influence of Hurricane Gloria (1985) on the environment has been evaluated by comparing the GFDL hurricane model integrations either including or excluding the hurricane in the initial conditions. Pairs of integrations were performed for three cases, each beginning at a different stage of the storm development.

This experimental design allowed the quantification of the magnitude and the areal extent of the cumulative impact of the hurricane on the environment since the initial time of the integration. The differences between the hurricane and nonhurricane integrations represented the hurricane's influence.

For each of the three cases presented here the area of negative sea level pressure differences (hurricane integration minus nonhurricane integration) initially associated with the direct presence/absence of the hurricane continuously expanded throughout the integration. The area covered by sea level pressure differences less than −1 hPa was used to define an effective influence radius of the storm. This influence radius eventually reached approximately 1500 km in each case in agreement with an estimate of the extent of hurricane influence (1600 km) obtained by Frank (1982) in a composite analysis study. Comparison of the sea level pressure difference fields for the three cases showed that the expansion rate of the hurricane's influence varied among the three cases. For example, in the first 60 h of integration, the case with the most intense storm expanded more rapidly than the case with the initially weakest storm. However, the relationship between the time series of the expansion rate and the intensity and intensity change of the storms (shown by the minimum surface pressure) is rather inconsistent. On the other hand, the extent of the sea level pressure differences for the three cases at the same verification time were much more similar than those extents after equal integration periods. This indicates that the differences are related to systematic modifications of the environment rather than a random divergence of the hurricane integration from the nonhurricane integration. It also suggests a possible controlling influence of the environment on the hurricane's evolution although this cannot be determined using the experimental strategy of this study.

A three-dimensional view of the hurricane's impact was obtained through analysis of the wind and temperature fields for the hurricane and nonhurricane integrations for the case with the most intense storm. It was shown that the hurricane's influence was far more extensive at the upper layer than at the lower layer. At the upper layer, a stronger anticyclonic circulation developed in the hurricane integration and the position of the anticyclone was shifted closer to the hurricane than that of the nonhurricane integration. A plausible explanation for the upper- and lower-layer wind speed difference patterns is the continued forcing by the hurricane's radial circulation, that is, low-level inflow and upper-level outflow, throughout the integration period. The temperature differences at the upper layer showed that the hurricane integration was warmer over an area comparable in size with the corresponding sea level pressure differences.

Although the area of the lower-layer differences in wind speed and temperature covered a smaller area than those at the upper layer, the lower-layer differences showed the impact of the hurricane on a particular synoptic feature, that is, a cold front to the west of the hurricane. Specifically, northwest of the hurricane, the passage of the cold front was delayed in the hurricane integration compared with the nonhurricane result because of the easterly component of the low-level cyclonic storm circulation. To the southwest of the storm, the hurricane circulation enhanced the westerly flow and hastened the passage of the front. The change in the speed of frontal movement resulted in a change in the precipitation pattern and in the lower-layer temperature distribution. In particular, to the southwest of the hurricane position, there was a reduction in the accumulated frontal precipitation in the hurricane integration because of the faster frontal movement.

This study has identified substantial changes in the environment because of the presence of a hurricane. The modified environment can in turn influence the storm motion, the structure of the storm and possibly even the evolution of other tropical disturbances within the influenced region. Modifications to the storm structure or motion may have occurred in the hurricane forecasts shown here, but it is not possible to isolate feedbacks from the environment to the hurricane with the present experimental strategy. However, the deep-layer mean wind is a quantity often used to derive the so-called steering current and can suggest the potential for feedback to the storm movement. Although the presented differences in the deep-layer mean winds between the hurricane and nonhurricane integrations were weaker than those at the upper layer, such a difference might have had an effect on the storm movement.

These results represent an example of environmental modification in the case of a particular storm. The specific difference patterns shown here may vary somewhat from case to case and are likely to depend on the particular large-scale environment as well as the hurricane structure and size. However, the general difference features linked to the hurricane's radial circulation, that is, stronger upper-level anticyclone, warmer upper-level temperatures, and lower sea level pressures, are likely to be found in other cases as well.

Acknowledgments. The authors are grateful to Jerry Mahlman, Morris A. Bender, and Robert E. Tuleya for their continuous encouragement during the course of the present study. They wish to thank Morris A. Bender for his considerable help in the assessment and analysis of the obtained results. They appreciate the constructive criticism and valuable suggestions of Morris A. Bender, Ronald Stouffer, and Chun-Chieh Wu on the original manuscript. Also they acknowledge the valuable comments by the reviewers that led to the clarification of certain issues and the significant improvement of the paper in general.

REFERENCES

Bender, M. A., R. E. Tuleya, and Y. Kurihara, 1987: A numerical study of the effect of island terrain on tropical cyclones. *Mon. Wea. Rev.*, **115,** 130–155.

——, R. J. Ross, R. E. Tuleya, and Y. Kurihara, 1993: Improvements in tropical cyclone track and intensity forecasts using the GFDL initialization system. *Mon. Wea. Rev.*, **121,** 2046–2061.

Frank, W. M., 1982: Large-scale characteristics of tropical cyclones. *Mon. Wea. Rev.*, **110,** 572–586.

Kurihara, Y., 1973: A scheme of moist convective adjustment. *Mon. Wea. Rev.*, **101,** 547–553.

——, and M. A. Bender, 1980: Use of a movable nested mesh model for tracking a small vortex. *Mon. Wea. Rev.*, **108,** 1792–1809.

——, ——, R. E. Tuleya, and R. J. Ross, 1990: Prediction experiments of Hurricane Gloria (1985) using a multiply-nested movable mesh model. *Mon. Wea. Rev.*, **118,** 2185–2198.

——, ——, and R. J. Ross, 1993: An initialization scheme of hurricane models by vortex specification. *Mon. Wea. Rev.*, **121,** 2030–2045.

Mellor, G. L., and T. Yamada, 1974: A hierarchy of turbulence closure models for planetary boundary layers. *J. Atmos. Sci.*, **31,** 1791–1806.

Molinari, J., and D. Vollaro, 1989: External influences on hurricane intensity. Part I: Outflow layer eddy angular momentum fluxes. *J. Atmos. Sci.*, **46,** 1093–1105.

Tuleya, R. E., 1994: Tropical storm development and decay: Sensitivity to surface boundary conditions. *Mon. Wea. Rev.*, **122,** 291–304.